Dissipative Scheme for Discontinuous Galerkin Time-Domain Method Based on a Leap-Frog Time-Stepping

Da Peng, Xingji Tang, Hu Yang, and Jianguo He

College of Electronic Science and Engineering
National University of Defense Technology, Changsha, 410073, China
da.peng.uestc@gmail.com, amani.11@163.com

Abstract ─ A dissipative scheme is proposed to improve numerical dispersion and eliminate spurious modes in the unstructured grid-based discontinuous Galerkin time-domain (DGTD) method. We introduce the dissipative terms into the centered fluxes, and a backward discretization in time is applied to the dissipative part to yield a fully explicit time-stepping scheme. In order to analyze the dispersion and dissipation properties of this scheme, we perform a numerical Fourier analysis to the normalized one-dimensional Maxwell's equations with periodic boundary conditions. In this process, the mechanism of suppression of the spurious modes is revealed for the dissipative scheme. Numerical results show that more accurate solutions can be obtained by using dissipative scheme in the DG method.

Index Terms – Backward discretization, centered fluxes, dissipative scheme, discontinuous Galerkin, fully explicit time-stepping, Fourier analysis, and periodic boundary conditions.

I. INTRODUCTION

Discontinuous Galerkin time-domain (DGTD) method is a novel numerical technique to solve time-dependent electromagnetic problems with complex geometries in which high accuracy and efficiency are required [1-4]. It employs discontinuous piecewise polynomials as basis and test functions, and then applies a Galerkin test procedure for each element to obtain the spatial discretization. The solutions are not enforced continuous across interface of any two adjacent elements. Instead, the unique fluxes are constructed to provide the coupling mechanism between elements, which gives rise to a highly parallel computation [5].

The centered fluxes coupled with a leap-frog time-stepping lead to a convergent, stable, and energy-conserving scheme [6, 12]. However, this scheme suffers from two problems: poor numerical dispersion properties and the existence of spurious modes. To improve numerical dispersion and eliminate spurious modes, a penalization of centered fluxes by dissipative terms is introduced to the DG method based on hexahedral elements [7]. With a mathematical analysis, it is shown in [7] that the dissipative scheme is less dispersive and has a better convergence than the non-dissipative one.

In practical DGTD models, the automatic mesh generation is often not feasible for building many 3D hexahedral meshes. The method of constructing an initial tetrahedral mesh and then splitting each cell into four hexahedral cells will generate a low-quality mesh [7, 8], and as a result a small time step is required due to the stability reasons. In this sense, an efficient algorithm based on tetrahedral elements may be more attractive for most problems of interest.

In this work, in order to decrease numerical dispersion error and eliminate spurious modes, the dissipative terms are introduced into the tetrahedron-based DG method as the penalization of centered fluxes. The construction of dissipative scheme is straightforward, and when employing the leap-frog algorithm, a backward discretization in time is applied to the dissipative terms to yield a fully explicit time-stepping scheme. This is distinguished from the way of directly using the upwind fluxes and employing a Runge-Kutta time-stepping method [1, 2, 10]. Numerical Fourier

Submitted On: Nov. 20, 2012
Accepted On: May 16, 2013

analysis of the fully discrete scheme is performed to investigate dispersion and dissipation relations with the mesh size per wave length. The related diagrams illustrate that the dissipative scheme is less dispersive and has the capability of suppressing spurious modes. Finally, the given examples, including metallic cavity and scattering problems, show that more accurate solutions can be obtained by using dissipative scheme in tetrahedron-based DGTD.

II. THEORY

A. Discontinuous Galerkin method

The time-domain Maxwell's curl equations for non-conducting dielectrics can be written in conservation form,

$$Q\frac{\partial \boldsymbol{q}}{\partial t}+\nabla\cdot\boldsymbol{F}=0, \tag{1}$$

where

$$Q=\begin{bmatrix}\mu & 0\\ 0 & \varepsilon\end{bmatrix},\quad \boldsymbol{q}=\begin{bmatrix}\boldsymbol{H}\\ \boldsymbol{E}\end{bmatrix},\quad \boldsymbol{F}=\begin{bmatrix}\boldsymbol{F}_H\\ \boldsymbol{F}_E\end{bmatrix}$$

and

$$\begin{bmatrix}\boldsymbol{F}_H^{\alpha}\\ \boldsymbol{F}_E^{\alpha}\end{bmatrix}=\left.\begin{bmatrix}\hat{\boldsymbol{n}}_{\alpha}\times\boldsymbol{E}\\ -\hat{\boldsymbol{n}}_{\alpha}\times\boldsymbol{H}\end{bmatrix}\right|_{\alpha=x,y,z}.$$

Here, ε and μ are respectively, the electric permittivity and magnetic permeability in materials, $\boldsymbol{E}$ and $\boldsymbol{H}$ are respectively, the electric and magnetic vector fields, $\hat{\boldsymbol{n}}_i$ signifies three Cartesian unit vectors. To solve a system of equations defined in equation (1) and pave the way for the nodal discontinuous Galerkin (DG) formulation, we assume that the computational domain Ω can be well approximated by a set Λ of non-overlapping elements $\left(\mathrm{D}^k\right)_{k=1\ldots K}$ .Define the following approximate space,

$$\mathrm{V}_h=\left\{\boldsymbol{v}(\boldsymbol{x})\in\left(L^2(\Omega)\right)^3:\forall k\in\Lambda,\boldsymbol{v}\big|_{\mathrm{D}^k}\circ\Im_k(\boldsymbol{\xi})\in\left(\mathrm{P}_p^3(\mathrm{I})\right)^3\right\}, \tag{2}$$

where $\circ$ denotes composition of functions, $\Im_k$ denotes the conform mapping $\Im_k:\mathrm{I}\to\mathrm{D}^k$, I is a standard tetrahedron defined by

$$\mathrm{I}=\left\{\boldsymbol{\xi}=(\xi,\eta,\zeta):(\xi,\eta,\zeta)\ge -1;\xi+\eta+\zeta\le -1\right\},$$

and $\mathrm{P}_p^3(\mathrm{I})$ represents the space of three-dimensional polynomials of maximum order p on the standard element I . We assume that we can approximate the solution $\boldsymbol{q}(\boldsymbol{x},t)$ by $\boldsymbol{q}_h(\boldsymbol{x},t)\in\left(\mathrm{V}_h\right)^2$. Within each element, we express $\boldsymbol{q}_h(\boldsymbol{x},t)$ in a nodal representation

$$\boldsymbol{q}_h^k(\boldsymbol{x},t)=\sum_{j=1}^{N}\boldsymbol{q}_j^k(t)L_j^k(\boldsymbol{x})=L_N^{\mathrm{T}}\boldsymbol{q}_N, \tag{3}$$

where $\boldsymbol{q}_j^k(t)$ denotes the discrete solution at space point $\boldsymbol{x}_j=\Im_k(\boldsymbol{\xi}_j)$, and $L_j^k(\boldsymbol{x})\in\mathrm{P}_p^3(\mathrm{D}^k)$ is the three-dimensional Lagrange interpolation polynomial based on N nodal points, $\boldsymbol{x}_j$, located in the interior as well as on the boundary of D^k . Furthermore, $\boldsymbol{q}_N=[\boldsymbol{q}_1^k,\ldots,\boldsymbol{q}_N^k]^{\mathrm{T}}$ and $L_N=[L_1^k(\boldsymbol{x}),\ldots,L_N^k(\boldsymbol{x})]^{\mathrm{T}}$ are the vector of the local nodal solution and the vector of Lagrange polynomials, respectively.

With the test functions $\phi_i(\boldsymbol{x})$, chosen to be the same as the basis functions $L_i(\boldsymbol{x})$, the approximate solution $\boldsymbol{q}_h$ is obtained by requiring the strong Galerkin formulation of equation (1) be satisfied over each element D^k

$$\int_{\mathrm{D}^k}\phi_i\left(Q\frac{\partial \boldsymbol{q}_h}{\partial t}+\nabla\cdot\boldsymbol{F}_h\right)d\boldsymbol{x}=\oint_{\partial\mathrm{D}^k}\phi_i\hat{\boldsymbol{n}}\cdot\left(\boldsymbol{F}_h-\boldsymbol{F}^*\right)d\boldsymbol{x}, \tag{4}$$

where $\partial\mathrm{D}^k$ is the boundary of element D^k , $\hat{\boldsymbol{n}}$ is the outward unit normal vector, and $\boldsymbol{F}^*$ is the numerical flux depends on the values of the tangential fields at both sides of $\partial\mathrm{D}^k$. Usually, for DG methods, a common choice of $\boldsymbol{F}_h^*$ is the centered flux

$$\hat{\boldsymbol{n}}\cdot\boldsymbol{F}^*=\frac{1}{2}\hat{\boldsymbol{n}}\times\begin{bmatrix}\boldsymbol{E}_h+\boldsymbol{E}_h^+\\ -(\boldsymbol{H}_h+\boldsymbol{H}_h^+)\end{bmatrix}, \tag{5}$$

where the superscript "+" refers to field values from the neighbour element.

Assuming that the materials are element wise constant, the matrix form for the semi-discrete scheme of equation (4) is obtained,

$$\begin{cases}\dfrac{d\boldsymbol{H}_N}{dt}=-\left(\mu\mathbf{M}\right)^{-1}\left(\mathbf{S}\times\boldsymbol{E}_N+\mathbf{F}\left(\hat{\boldsymbol{n}}_N\times\left(\dfrac{\boldsymbol{E}_N^+-\boldsymbol{E}_N}{2}\right)\right)\Big|_{\partial\mathrm{D}^k}\right)\\ \dfrac{d\boldsymbol{E}_N}{dt}=\left(\varepsilon\mathbf{M}\right)^{-1}\left(\mathbf{S}\times\boldsymbol{H}_N+\mathbf{F}\left(\hat{\boldsymbol{n}}_N\times\left(\dfrac{\boldsymbol{H}_N^+-\boldsymbol{H}_N}{2}\right)\right)\Big|_{\partial\mathrm{D}^k}\right),\end{cases} \tag{6}$$

where

$$\mathbf{M}_{ij} = \int_{\mathrm{D}^k} L_i(\boldsymbol{x}) L_j(\boldsymbol{x}) d\boldsymbol{x},$$
$$\mathbf{S}_{ij} = \int_{\mathrm{D}^k} L_i(\boldsymbol{x}) \nabla L_j(\boldsymbol{x}) d\boldsymbol{x},$$
$$\mathbf{F}_{il} = \int_{\partial \mathrm{D}^k} L_i(\boldsymbol{x}) L_l(\boldsymbol{x}) d\boldsymbol{s}$$

are the local mass, stiffness, and face-based mass matrices and the vectors of the local nodal solution unknowns, respectively. Since a conform mapping $\Im_K$ existed between elements D^k and I, these matrices can be conveniently constructed using the corresponding template matrices defined on I. It saves not only preprocessing time but also reduces the required storage very substantially. Efficient and accurate implementation techniques have been discussed in [1] in detail.

B. Penalization of centered flux

It is already known for time-domain problems that the centered flux can result in a non-dissipative system when combined with a leap-frog time integration scheme, where the electric fields are evaluated at the time $n\Delta t$ and the magnetic fields at the time $(n+0.5)\Delta t$. Unfortunately, the DG method based on totally centered fluxes will generate numerical spurious modes, which degrades the accuracy of the solution.

Inspired by the work of E. Montseny et al [7], we introduce a penalization of the centered flux by some dissipative terms into the nodal DG method based on tetrahedral grids. Adding the dissipative terms in the numerical scheme, the new formulation of the problem on each element becomes

$$\begin{cases} \dfrac{d\boldsymbol{H}_N}{dt} = -(\mu\mathbf{M})^{-1}\left(\mathbf{S}\times\boldsymbol{E}_N + \mathbf{F}\left(\hat{\boldsymbol{n}}_N \times \left(\dfrac{\boldsymbol{E}_N^+ - \boldsymbol{E}_N}{2} + \hat{\boldsymbol{n}}_N \times \dfrac{\boldsymbol{H}_N^+ - \boldsymbol{H}_N}{\lambda_H} \right) \right)\Big|_{\partial \mathrm{D}^k} \right) \\ \dfrac{d\boldsymbol{E}_N}{dt} = (\varepsilon\mathbf{M})^{-1}\left(\mathbf{S}\times\boldsymbol{H}_N + \mathbf{F}\left(\hat{\boldsymbol{n}}_N \times \left(\dfrac{\boldsymbol{H}_N^+ - \boldsymbol{H}_N}{2} - \hat{\boldsymbol{n}}_N \times \dfrac{\boldsymbol{E}_N^+ - \boldsymbol{E}_N}{\lambda_E} \right) \right)\Big|_{\partial \mathrm{D}^k} \right) \end{cases} \tag{7}$$

where $\lambda_E = \sqrt{\mu/\varepsilon} + \sqrt{\mu^+/\varepsilon^+}$ and $\lambda_H = \sqrt{\varepsilon/\mu} + \sqrt{\varepsilon^+/\mu^+}$. Note that this is very similar with the upwind flux [1, 2, 10, 13]. For the time derivatives in equation (7), the classical leap-frog method will lead to a globally implicit time-scheme, which is very expensive to execute for computer. Alternatively, if the penalization terms are approximated in time by a backward discretization, a fully explicit time integration scheme can be obtained,

$$\begin{cases} \dfrac{\boldsymbol{H}_N^{n+1/2} - \boldsymbol{H}_N^{n-1/2}}{dt} = -(\mu\mathbf{M})^{-1}\left(\mathbf{S}\times\boldsymbol{E}_N^n + \mathbf{F}\left(\hat{\boldsymbol{n}}_N \times \left(\dfrac{\left(\boldsymbol{E}_N^+ - \boldsymbol{E}_N\right)^n}{2} + \hat{\boldsymbol{n}}_N \times \dfrac{\left(\boldsymbol{H}_N^+ - \boldsymbol{H}_N\right)^{n-1/2}}{\lambda_H} \right)\Big|_{\partial \mathrm{D}^k} \right) \right) \\ \dfrac{\boldsymbol{E}_N^{n+1} - \boldsymbol{E}_N^n}{dt} = (\varepsilon\mathbf{M})^{-1}\left(\mathbf{S}\times\boldsymbol{H}_N^{n+1/2} + \mathbf{F}\left(\hat{\boldsymbol{n}}_N \times \left(\dfrac{\left(\boldsymbol{H}_N^+ - \boldsymbol{H}_N\right)^{n+1/2}}{2} - \hat{\boldsymbol{n}}_N \times \dfrac{\left(\boldsymbol{E}_N^+ - \boldsymbol{E}_N\right)^n}{\lambda_E} \right)\Big|_{\partial \mathrm{D}^k} \right) \right) \end{cases}. \tag{8}$$

Reference [7] has proven that the backward discretization for the time approximation of penalization terms leads to slightly more restrictive stability condition than the one obtained with the complete centered scheme. This means that more integration steps are needed to simulate the previous time.

C. Dispersive and dissipative properties

Fourier analysis [10] is carried out to investigate the dispersion and dissipation behavior of numerical scheme defined in section B. By introducing the normalized quantities $\tilde{\boldsymbol{x}} = \boldsymbol{x}/L$ and $\tilde{t} = t/(L/c_0)$, where L is a reference length and $c_0 = 1/\sqrt{\varepsilon_0\mu_0}$ represents the dimensional speed of light in vacuum, the fields are made non-dimensional as,

$$\tilde{\boldsymbol{H}} = \frac{\boldsymbol{H}}{H_0}, \quad \tilde{\boldsymbol{E}} = \frac{\boldsymbol{E}}{Z_0 H_0}, \quad \tilde{\boldsymbol{J}} = \frac{\boldsymbol{J}}{H_0/L}.$$

Here $Z_0 = \sqrt{\mu_0/\varepsilon_0}$ is the free-space intrinsic impedance and H_0 is a reference magnetic field strength. Then, we take the normalized one-dimensional formulation

$$\begin{cases} \dfrac{d\tilde{H}_N^z}{d\tilde{t}} = \mathbf{M}^{-1}\begin{pmatrix} -\mathbf{S}\tilde{E}_N^y + \dfrac{e_N}{2}\left(\tilde{E}_N^y - \tilde{E}_N^{y^+} - (1-\alpha)(\tilde{H}_N^z - \tilde{H}_N^{z^+}) \right)_{x_r} \\ -\dfrac{e_0}{2}\left(\tilde{E}_N^y - \tilde{E}_N^{y^+} + (1-\alpha)(\tilde{H}_N^z - \tilde{H}_N^{z^+}) \right)_{x_l} \end{pmatrix} \\ \dfrac{d\tilde{E}_N^y}{d\tilde{t}} = \mathbf{M}^{-1}\begin{pmatrix} -\mathbf{S}\tilde{H}_N^z + \dfrac{e_N}{2}\left(\tilde{H}_N^z - \tilde{H}_N^{z^+} - (1-\alpha)(\tilde{E}_N^y - \tilde{E}_N^{y^+}) \right)_{x_r} \\ -\dfrac{e_0}{2}\left(\tilde{H}_N^z - \tilde{H}_N^{z^+} + (1-\alpha)(\tilde{E}_N^y - \tilde{E}_N^{y^+}) \right)_{x_l} \end{pmatrix} \end{cases} \tag{9}$$

where $x \in [x_l, x_r]$ and e_i is a N long zero vector with 1 in entry i. If $\alpha = 1$, the scheme is non-dissipative, corresponding to the semi-discrete

system in equation (6). For $\alpha = 0$, it yields a dissipative scheme corresponding to equation (7).

Consider propagation of a monochromatic plane wave $e^{j(kx-\omega t)}$. If the periodic boundary conditions (PBC)

$$(u^+)_{x_r} = e^{jkh}(u)_{x_l}, \quad (u^+)_{x_l} = e^{-jkh}(u)_{x_r} \tag{10}$$

are enforced in equation (9), where $h = x_r - x_l$ and k now is the wavenumber, then the space discretized system in equation (9) can be expressed as,

$$\frac{\partial}{\partial t}\begin{bmatrix} \tilde{H}_N^z \\ \tilde{E}_N^y \end{bmatrix} = \begin{bmatrix} A_{hh} & A_{he} \\ A_{eh} & A_{ee} \end{bmatrix}\begin{bmatrix} \tilde{H}_N^z \\ \tilde{E}_N^y \end{bmatrix}. \tag{11}$$

Here A_{ee}, A_{eh}, A_{he} and A_{hh} are $N \times N$ matrices, the expressions of which are straightforward but somewhat lengthy. For the non-dimensional form of Maxwell's equations, the analytic dispersion relation is $k^2 = \omega^2$. In order to investigate numerical dispersion relationship for this fully discrete scheme, we introduce the numerical wave frequency $\tilde{\omega}$ and expect it to satisfy,

$$\begin{bmatrix} \tilde{H}_N^{z\ n+1/2} \\ \tilde{E}_N^{y\ n+1} \end{bmatrix} = e^{-j\tilde{\omega}\Delta t}\begin{bmatrix} \tilde{H}_N^{z\ n-1/2} \\ \tilde{E}_N^{y\ n} \end{bmatrix}. \tag{12}$$

In addition, we can write equation (11) as a fully explicit scheme by a backward discretized approximation in time

$$\begin{bmatrix} \tilde{H}_N^{z\ n+1/2} \\ \tilde{E}_N^{y\ n+1} \end{bmatrix} = B\begin{bmatrix} \tilde{H}_N^{z\ n-1/2} \\ \tilde{E}_N^{y\ n} \end{bmatrix}, \tag{13}$$

and

$$B = \begin{bmatrix} I + \Delta t A_{hh} & \Delta t A_{he} \\ \Delta t A_{eh}(I + \Delta t A_{hh}) & I + \Delta t A_{ee} + \Delta t^2 A_{eh} A_{he} \end{bmatrix},$$

where I is the $N \times N$ identity matrix. Substituting equation (12) into equation (13), we obtain the eigenvalue problem,

$$e^{-j\tilde{\omega}\Delta t}\begin{bmatrix} \tilde{H}_N^{z\ n-1/2} \\ \tilde{E}_N^{y\ n} \end{bmatrix} = B\begin{bmatrix} \tilde{H}_N^{z\ n-1/2} \\ \tilde{E}_N^{y\ n} \end{bmatrix}. \tag{14}$$

Solving this eigenvalue equation will produce $2N$ different values for $\tilde{\omega}_n = \tilde{\omega}_n^r + j\tilde{\omega}_n^i$. This is because an infinite set of real wavenumbers $\pm k_n$ satisfying

$$k_n = k + 2n\pi / h, \quad n = 0, \pm 1, \pm 2, \ldots \tag{15}$$

are also supported by the periodic boundary conditions in equation (10). We will refer to $\pm k_0$ as the fundamental modes while to the others as harmonic modes.

Assume that second-order polynomials are applied for the spatial discretization ($p = 2$), and for the time discretization we use

$$\Delta t = \frac{C}{2p+1} \cdot \frac{h}{p+1}, \tag{16}$$

as the time step size, which is equivalent to the setting in the $p+1$ order SSP-RK scheme [10]. The dispersion relations for the two schemes (i.e., dissipative and non-dissipative) are shown in Figs. 1 and 2, respectively. We see that for $L \ll 1$, only the numerical phase velocity of $\pm\tilde{k}_0$ is very close to the physical wave speed, but the other modes present undesired behavior on the phase speed due to the coarse discretization. These modes, which do not properly approximate any analytical one over intervals of L are treated as spurious or non-physical modes [9]. Furthermore, we also see that for the dissipative scheme, a better approximation of fundamental modes over more bandwidth is achieved than for the non-dissipative one, which exhibits unphysical behavior for the phase speed even in the well-resolved case of $L \simeq \pi / 4$.

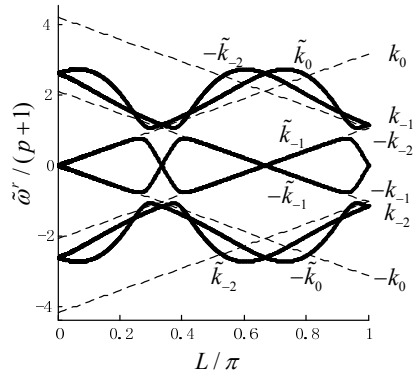

Fig. 1. Numerical dispersion relations for non-dissipative scheme of one-dimensional DGTD, $L = kh/(p+1)$, $C = h = 1$. The dashed lines represent analytical dispersion curves (equation (15)) and the solid lines reflect the dispersion characteristics for numerical modes.

For the non-dissipative scheme, the numerical modes do not attenuate in any case ($\tilde{\omega}_n^i = 0$), so the harmonics may appear together with fundamental modes in a simulation. In contrast to this, we also show in Fig. 2 the imaginary parts of all six modes for the dissipative scheme. We see

that the spurious modes are severely damped but the fundamental modes (or physical modes) are almost reserved in the interval $L<\pi/3$. This means the suppression of numerical spurious modes.

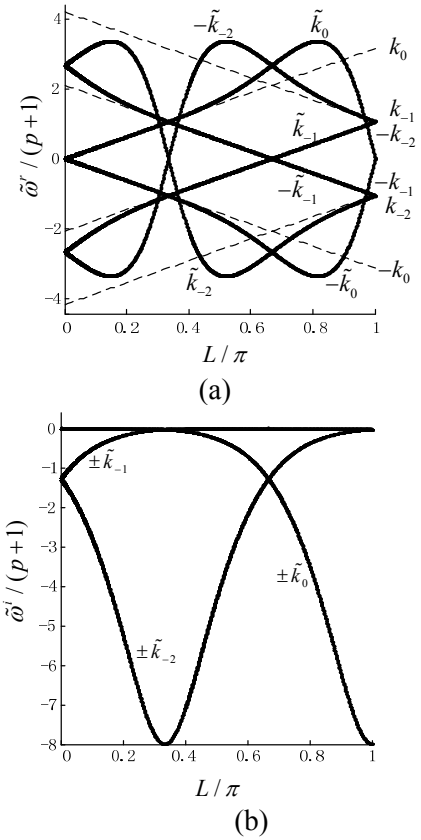

Fig. 2. Numerical dispersion (a) and dissipation (b) relations for the dissipative scheme of one-dimensional DGTD, $L=kh/(p+1)$, $C=h=1$. The solid lines reflect the dispersion or dissipation characteristics for numerical modes.

III. NUMERICAL RESULTS

To demonstrate the advantages of taking into account the dissipative terms in our scheme, we first consider the one-dimensional metallic cavity problem in the domain $x\in[-1,1]$ filled with vacuum, whose analytical solution is given by,

$$\begin{cases}\tilde{E}_y=\sin(\omega x)\sin(\omega t)\\ \tilde{H}_z=\cos(\omega x)\cos(\omega t)\end{cases} \tag{17}$$

with $\omega=n\pi$ ($n\in\mathbb{N}^+$). We choose $n=2$ and excite metallic cavity with the values at time $t=0$. There is no spurious mode arising due to this initial values setting. Figure 3 shows comparison on accuracy between the solutions obtained with the two schemes at $x=0$ in a long integration time equivalent to 40 wavelengths (only a portion of the time range is displayed in Fig. 3). Considering the backward discretization in time for the penalization terms, we restrict the time step size by $C=0.6$.

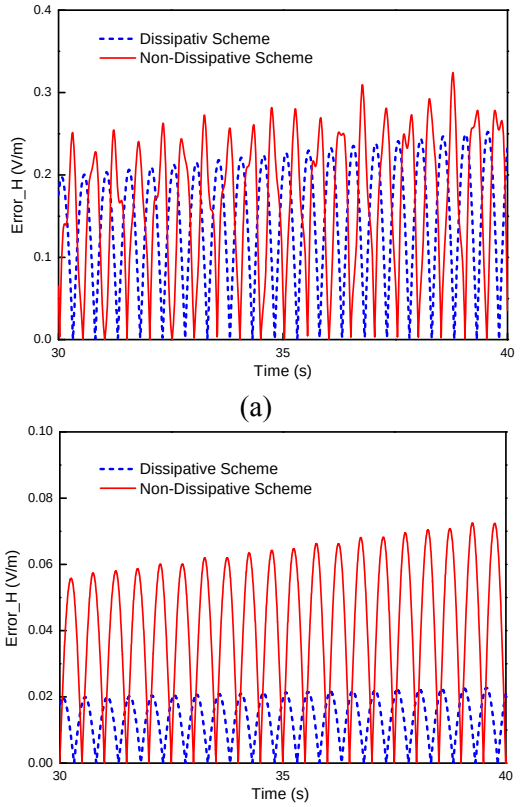

Fig. 3. Comparison on accuracy for two schemes, (a) $p=2$ with 8 equidistant elements (b) $p=4$ with 4 equidistant elements.

We note the advantage of the dissipative approach in the figure above. This benefit is mainly due to the less dispersive error than that of the non-dissipative approach. For example, in the case of $p=4$ and $K=4$, the numerical phase velocities, which can be measured by the locations of the zero crossings (in Fig. 4) are 1.0000495 and 1.0002971 for the dissipative and the non-dissipative approaches, respectively. In fact, for the dissipative scheme in Fig. 3, an important part

of the errors come from the decrease in amplitude with time ($\tilde{\omega}^i$ <0). An FDTD solution with a cell size of $\lambda/40$ is added for comparison, the numerical phase velocity of which is only 0.9989985. Furthermore, we compare results obtained with the FDTD and DG methods in Table 1. The improvement is expressed in terms of storage, CPU time and the L^2 errors, which defines the L^2 norm of the difference between the exact solution and the solutions computed for each degree of freedom (DOF) in this problem at time $t = 40$. Both DGTD approaches outperform traditional FDTD in accuracy and memory usage. It can be seen from Table 1 that the dissipative scheme is more accurate than the non-dissipative one, but more time-consuming due to the rigorous restriction on stability and the extra operations to implement the dissipative terms. How to reduce the time cost of dissipative scheme is beyond the scope of this study, and will be addressed elsewhere in the future.

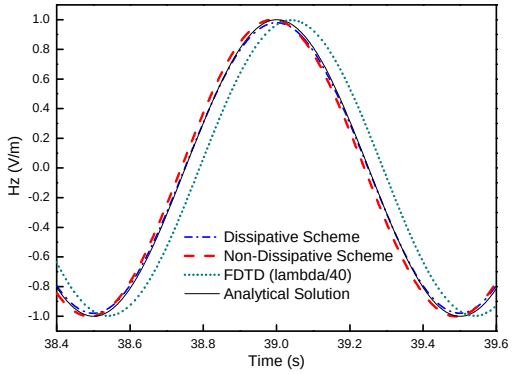

Fig. 4. Comparison of DG/FDTD results at the center of the cavity ($p = 4$ with 4 equidistant elements).

Table 1: DOF, L^2 error and CPU time costs at $t = 40$.

Method	DGTD $p = 4$, $K = 4$		FDTD $\lambda/40$
	non-dissipative	dissipative	
DOF	40	40	161
L^2 error	0.22	0.09	1.51
CPU (s)	0.88	1.16	0.455

The second example is to model the scattering of electromagnetic waves from a PEC sphere of radius $a = 10/2\pi$, whose analytical solution can be achieved with infinite series of Legendre and spherical Hankel functions [11]. The sphere is illuminated by a plane wave given by $\hat{k}_{inc} = (0,0,1)$ and $E_x(t) = \exp(-4\pi\left(\frac{t - 4.466\times10^{-9}}{2.233\times10^{-9}}\right)^2)$. The mesh size on the surface of the sphere is 0.3 m. One observation point is located outside the sphere at (0,0,-2.2) m (the origin is at the sphere center). In Fig. 5, we compare the results obtained by using or not the dissipative terms in the DG formulation. We can see the former scheme leads to a more accurate solution than the scheme without dissipative terms at the same spatial order ($p = 2$). Little oscillation appears in the solution of the latter scheme, which certainly due to the propagation of spurious modes [7]. The use of higher order ($p = 3$) in the non-dissipative scheme improves the solution but executes approximately 4.7 times slower with a 100 % increase in the required memory. The E-plane bistatic cross sections obtained from the same calculation for $ka = 10$ ($f = 300$ MHz) are also shown in Fig. 6. It is in good agreement with the exact solution.

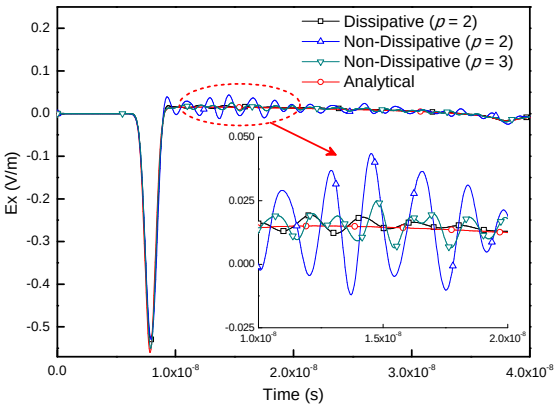

Fig. 5. Electric fields located at (0,0,-2.2) m.

The above example is not a difficult test case since the geometry of the sphere is simple and the unstructured high-quality meshes can be built with little difficulties. For complex problems, strong size-disparities and cell-distortions are usually observed in the meshes, based on which it is easier to generate numerical spurious modes for the non-dissipative scheme. The following example shows it is necessary to import the dissipative terms in

our DG scheme to obtain more accurate solutions with low spatial order approximation.

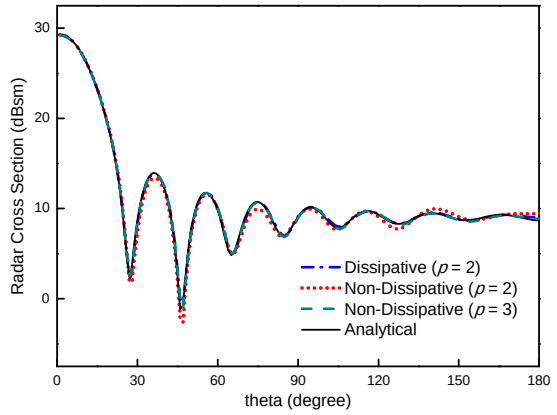

Fig. 6. Bistatic RCS for metallic sphere of $ka = 10$.

We consider plane wave scattering by a generic missile. As illustrated in Fig. 7, the thin wings of thickness 0.005 m have to be approximated by a small part of tetrahedrons with a large aspect ratio. The plane wave is given by $\hat{k}_{inc} = (0,0,-1)$ and $E_x(t) = \exp(-4\pi\left(\frac{t - 4.466\times10^{-10}}{2.233\times10^{-10}}\right)^2)$. The average mesh size on the surface of the missile is 0.02 m (1/5 wavelength at frequency 3 GHz). One observation point is located at a distance of 0.01 m from the top of the missile. Different solutions are obtained with the dissipative and non-dissipative DG methods, respectively. An FDTD solution with a cell size of 0.0025 m has been obtained as the reference solution. We can see the similar oscillation appears in the non-dissipative scheme while a convergent solution is achieved in the dissipative one. The *E*-plane bistatic cross sections obtained from the same calculation are shown in Fig. 9. It is in good agreement with the refined FDTD solution.

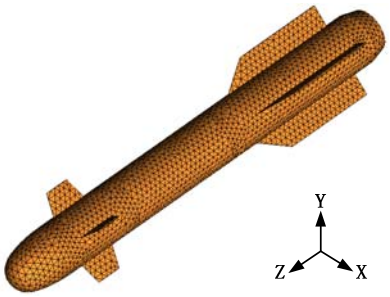

Fig. 7. Surface mesh for a generic missile.

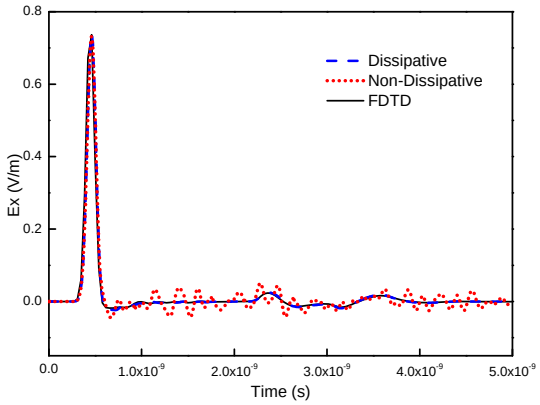

Fig. 8. Electric fields located at a distance of 0.01 m from the top of the missile ($p = 2$).

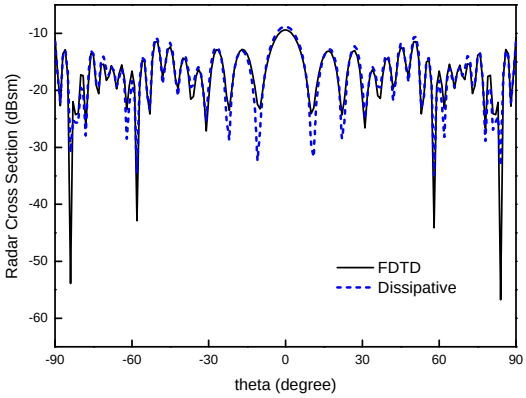

Fig. 9. Bistatic RCS of metallic missile ($p = 2$).

IV. CONCLUSION

Compared with the method proposed in [7], it is often more convenient to capture fine geometrical details of objects for the tetrahedron-based DG algorithm. In this paper, a dissipative scheme has been introduced to improve numerical dispersion and eliminate spurious modes in the tetrahedron-based DG method. We introduce the dissipative terms into the centered fluxes, and a backward discretization in time is applied to the dissipative part to yield a fully explicit time-stepping scheme. In order to analyze the dispersion and dissipation properties of this scheme, a numerical Fourier analysis is performed to the normalized 1-D Maxwell's equations with periodic boundary conditions. In this process, the mechanism of suppression of the spurious modes is revealed for the dissipative scheme. Some examples are given in the end. It shows that more accurate solutions can be obtained by using dissipative scheme in tetrahedron-based DGTD.

ACKNOWLEDGMENT

This work was supported by the National Science Foundation through grant No. 61171016.

REFERENCES

[1] J. S. Hesthaven and T. Warburton, "Nodal high-order methods on unstructured grids. I. time-domain solution of Maxwell's equations," *J. Comput. Phys.*, vol. 181, no. 1, pp. 186-221, 2002.

[2] J. S. Hesthaven and T. Warburton, *Nodal Discontinuous Galerkin Methods: Algorithms, Analysis, and Applications*, Springer, New York, 2007.

[3] M. Klemm, S. Lanteri, and C. Scheid, "Development of a DGTD method for dispersive media," *28th Annual Review of Progress in Applied Computational Electromagnetics (ACES)*, pp. 1064-1069, Columbus, Ohio, April 2012.

[4] K. Sirenko, M. Liu, and H. Bagci, "Accurate solution of Maxwell equations with exact absorbing boundary conditions for 2-D waveguide problems using time-domain discontinuous Galerkin finite element method," *28th Annual Review of Progress in Applied Computational Electromagnetics (ACES)*, pp. 1014-1018, Columbus, Ohio, April 2012.

[5] S. Dosopoulos and J. Lee, "A parallel and non-conformal interior penalty discontinuous Galerkin method for the time-domain Maxwell`s equations," *28th Annual Review of Progress in Applied Computational Electromagnetics (ACES)*, pp. 1040-1045, Columbus, Ohio, April 2012.

[6] S. Piperno and L. Fezoui, "A centered discontinuous Galerkin finite volume scheme for the 3D heterogeneous Maxwell equations on unstructured meshes," *INRIA Research Report*, no. 4733, 2003.

[7] E. Montseny, S. Pernet, X. Ferriéres, and G. Cohen, "Dissipative terms and local time-stepping improvements in a spatial high order discontinuous Galerkin scheme for the time-domain Maxwell's equations," *J. Comput. Phys.*, vol. 227, pp. 6795-6820, 2008.

[8] G. Cohen, X. Ferriéres and S. Pernet, "A spatial high-order hexahedral discontinuous Galerkin method to solve Maxwell's equations in time domain," *J. Comput. Phys.*, vol. 217, pp. 340-363, 2006.

[9] J. Alvarez, L. D. Angulo, A. R. Bretones, and S. G. Garcia, "A Spurious-free discontinuous Galerkin time-domain method for the accurate modeling of microwave filters," *IEEE Trans. Microw. Theory Tech.*, vol. 60, no. 8, pp. 2359-2369, Aug. 2008.

[10] D. Sármány, M. A. Botchev, and J. J. W. van der Vegt, "Dispersion and dissipation error in high-order Runge-Kutta discontinuous Galerkin discretizations of the Maxwell equations," *J. Sci. Comput.*, vol. 33, pp. 47-74, 2007.

[11] G. T. Ruck, D. E. Barrick, W. D. Stuart, and C. K. Krichbaum, *Radar Cross Section Handbook*, Plenum Press, New York, 1970.

[12] L. Fezoui, S. Lanteri, S. Lohrengel, and S. Piperno, "Convergence and stability of a discontinuous Galerkin time-domain method for the 3D heterogeneous Maxwell equations on unstructured meshes," *ESAIM Math. Model. Numer. Anal.*, vol. 39, no. 6, pp. 1149-1176, 2005.

[13] A. H. Mohammadian, V. Shankar, and W. F. Hall, "Computation of electromagnetic scattering and radiation using a time-domain finite-volume discretization procedure," *Computer Physics Communications*, vol. 68, pp. 175-196, 1991.

Da Peng received the B.Sc. degree in Electrical Engineering from the University of Electronic Science and Technology of China, Chengdu, China, in 2006, the M.Sc. degree in Electrical Science and Technology from the National University of Defense Technology, Changsha, China, in 2008. His primary interests include computational electrodynamics in the TD, finite element methods, and method of moments in the FD, and the application of numerical techniques for antenna and scattering problems.

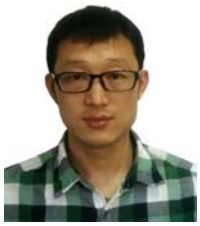

Xingji Tang received the B.Sc. and M.Sc. degrees in Electrical Science and Technology from the National University of Defense Technology, Changsha, China, in 2007 and 2009, respectively. He has been involved with shooting and bouncing ray tracing method applied to electromagnetic scattering analysis for electrically large structures.

Hu Yang received the Ph.D. degree in Electrical Science and Technology from the National University of Defense Technology, Changsha, China, in 2007. He is presently a Full Professor with National University of Defense Technology. His research interests include computational electromagnetics, microwave imaging and sensing (Synthetic Aperture Radar, SAR) and antenna design.